# Vibrational and Rotational Excitation and Relaxation of Nitrogen from Accurate Theoretical Calculations

Richard Jaffe[2], David W. Schwenke[3], Galina Chaban[4]
*NASA Ames Research Center*
*Moffett Field, CA 94035-1000*

*and*

Winifred Huo[5]
*Huo Consulting, LLC*
*Los Altos, CA 94024-3168*

**Vibrational and rotational energy transfer rate coefficients are computed for high-temperature $N_2$ under conditions expected for re-entry into Earth's atmosphere at 10-12 km/s. The calculations utilized classical mechanics to simulate individual collisions of $N_2$ with N atoms and a quantum chemical potential energy surface to describe the interatomic forces between the nitrogen atoms. The results demonstrate the importance of exchange reactions, which result in multiquantum jumps in vibration and rotation level.**

## Nomenclature

| | | |
|---|---|---|
| A | = | pre-exponetial parameter in Arrhenius expression for reaction rate coefficient |
| $D_e$ | = | diatomic molecule dissociation energy (measured from the bottom of the potential well) |
| E | = | total electronic energy in the solution of the Schrödinger equation. |
| $E_A$ | = | activation energy in Arrhenius expression for reaction rate coefficient |
| $E_{rel}$ | = | relative collision energy |
| $E_{vib}$ | = | average vibrational energy |
| H | = | Hamiltonian operator in the Schrödinger equation |
| J | =. | initial rotation quantum number |
| J' | = | final rotation quantum number |
| K | = | reaction rate coefficient |
| $k_B$ | = | Boltzmann constant |
| n | = | temperature-dependence parameter in Arrhenius expression for reaction rate coefficient |
| N | = | nitrogen atom |
| $N^a$, $N^b$, $N^c$ | = | labels for specific nitrogen atoms in $N_3$ |
| $N_2$ | = | diatomic (molecular) nitrogen |
| $N_3$ | = | the set of 3 nitrogen atoms to describe the $N_2$ + N collisions |
| R | = | separation between atoms in a diatomic molecule |
| $R_e$ | = | equilibrium bond distance in a diatomic molecule |
| S | = | collision cross section |
| t | = | time |
| $T_{ave}$ | = | average temperature in 2-T models |
| $T_{electron}$ | = | electron temperature |
| $T_{electronic}$ | = | electronic state temperature |

---

[2] Research Scientist, Nanotechnology Branch, Mail Stop 230-3, Member AIAA.
[3] Research Scientist, Application Branch, Mail Stop 230-3, Member AIAA.
[4] Research Scientist, Application Branch.
[5] Principal Scientist, Huo Consulting LLC, 680 Blinn Court, Member AIAA.

| $T_{int}$ | = | internal temperature (i.e., vibration plus rotation) |
|---|---|---|
| $T_{kin}$ | = | kinetic temperature |
| $T_{rot}$ | = | rotational temperature |
| $T_{vib}$ | = | vibrational temperature |
| v | = | initial vibration quantum number |
| v' | = | final vibration quantum number |
| dE | = | estimated error in the computed potential energy from quantum chemistry |
| DJ | = | change in rotation quantum number as a result of a collision |
| Dv | = | change in vibration quantum number as a result of a collision |
| $t_{rot}$ | = | rotational relaxation time |
| $t_{vib}$ | = | vibrational relaxation time |
| Y | = | wavefunction in the Schrödinger equation |

# I. Introduction

There has been considerable interest in understanding the physics and chemistry of shock heated air formed around a body during high-speed entry into Earth's atmosphere. For high entry velocities and at high altitudes, there are not enough collisions between gaseous species to maintain a state of chemical and thermodynamic equilibrium throughout this shock layer. One consequence of this nonequilibrium condition is an increase in radiation from the hot gas that increases the heat flux experienced by the body. For lunar or mars return missions, the entry velocity will exceed 10 km/s and radiative heating will be a significant contributor to the heat load experienced by the spacecraft.

A full characterization of the nonequilibrium gas requires detailed accounting of the distribution of rotation-vibration levels and electronic states of the air species. Much of the previous work in this area, by Park[1-4], Losev et al.[5] and others, has simplified the description of this nonequilibrium condition by using a two-temperature model based on distinct gas kinetic or translation ($T_{kin}$) and vibration ($T_{vib}$) temperatures. For these so called 2-T models, it is assumed that the molecular rotation energy distribution is in equilibrium with translation energy ($T_{rot} = T_{kin}$) and that the electronic state distribution and free electron energy are in equilibrium with vibration energy ($T_{electronic} = T_{electron} = T_{vib}$). $T_{kin}$ is governed by overall mass, energy and momentum conservation relationships and $T_{vib}$ is controlled by a separate relaxation/excitation rate,

$$\frac{dE_{vib}(T_{vib})}{dt} = \frac{d[E_{vib}(T) - E_{vib}(T_{vib})]}{\tau_{vib}} \qquad (1)$$

where $t_{vib}$ is the vibrational relaxation time (the characteristic time for a diatomic molecule to undergo a transition from v = 1 → 0). $t_{vib}$ is related to the vibrational relaxation rate coefficient (K(1 → 0)), which can be computed from the Landau-Teller [6], Schwartz, Slawsky and Herzfeld (SSH)[7], or Forced Harmonic Oscillator (FHO)[8] models. These models have been derived for a nonrotating harmonic oscillator and a simple repulsive potential with parameters adjusted to reproduce experimentally determined relaxation times. The FHO-FR model [9] has also been used. It extends the FHO model for two rotating harmonic oscillators but still uses an overly simplified interaction potential. The rationale for assuming $T_{rot} = T_{kin}$ and $T_{vib} \neq T_{kin}$ is that, at moderate temperatures (generally <5000 K), the rotation population in a gas is equilibrated after a small number of collisions, while equilibration of the vibration population requires $\sim 10^3$ collisions. Data for parameterizing rotational and vibrational relaxation times have generally come from shocktube experiments at temperatures of 5000-10,000 K, but the model is commonly extrapolated to 20,000 K or higher. For vibration, the curvefits of Millikan and White[10] are generally used for this purpose. The 2-T model of Park has been widely accepted by the aerothermodynamics community and has been continually updated as better experimental and theoretical data became available. However, Giordano[11] recently proposed a different 2-T model that uses the internal temperature ($T_{int}$) instead of the vibration temperature. In this formulation, rotation and vibration modes are coupled and the population of rotation-vibration levels is characterized by $T_{int}$. These 2-T models have been validated by comparison with flight data from Apollo and space shuttle missions and with ground-based data from shocktube experiments and arcjet tests, but many of their basic assumptions of all these 2-T models have not been rigorously tested.

The extent of diatomic-molecule dissociation and electronic excitation and ionization of the air species is sensitive to the distribution of energy between the modes characterized by these two temperatures. Initially in the shock layer, $T_{kin}$ spikes at 20,000 K or higher and then falls off to a thermal equilibrium temperature, which is generally between 7500 and 12,500 K. Simultaneously, $T_{vib}$ rises gradually to this equilibrium temperature (c.f., [4]). This is illustrated schematically in Fig. 1. The part of the shock layer where $T_{kin} > T_{vib}$ is called the thermal nonequilibium region and is where most of the conversion of the ambient air ($N_2$ and $O_2$) to N, O, $N^+$, $O^+$ and NO takes place. The temperature is determined from the ratio of low-lying energy levels and there is almost no information as to whether populations of high-lying levels are depleted from their Boltzmann values. While the "temperature" of an energy mode like rotation or vibration is dominated by the population of the lower or moderate energy levels, reaction rates for dissociation are more dependent on the population of high-lying levels. Therefore, deviation of high-lying levels from Boltzmann populations can have a significant effect on the dissociation rate. For example, using a 2-T model with $T_{rot} = T_{kin}$, $N_2$ and $O_2$ will appear to dissociate faster after passing through the shock (because of the spike in $T_{kin}$) then it should if the high-lying rotation level populations are depleted from their Boltzmann values.
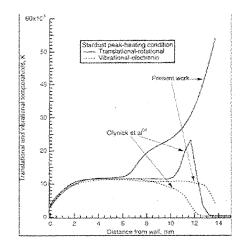


**Figure 1. Predicted temperature profiles for peak heating point on Stardust return trajectory from [4]. The shock is 13 cm in front of the capsule. Two separate predictions (by Park and Olynick) are shown, both exhibit translational-rotational temperature in excess of 20,000 K (solid lines) and vibrational temperature (dotted lines) that rises to 11,000 K.**

In Park's 2-T model[1-4], the chemical reaction rates are dependent on a geometric average temperature

$$T_{ave} = T_{kin}^{s} T_{vib}^{1-s} \tag{2}$$

where s is between 0.5 and 0.7[12] and the reaction rate coefficients are expressed as

$$K(T_{kin}, T_{vib}) = A T_{ave}^{n} \exp(-E_A / k_B T_{ave}) \tag{3}$$

The dissociation rates of $N_2$ and $O_2$ are sensitive to the value of $T_{rot}$ in the non-equilibrium model, because the effective dissociation energy of a diatomic molecule decreases as the rotation energy increases. As illustrated in Fig. 2, when a diatomic molecule rotates the centrifugal force perturbs the rotationless potential energy curve (resulting in a term $\sim J(J+1)/R^2$ being adding to the potential). As the rotation quantum number J increases, the bond energy decreases and an energy barrier to dissociation forms and becomes larger.[13,14] For sufficiently large J, the potential becomes completely repulsive. Thus, if $T_{rot}=T_{kin}$, diatomic molecule dissociation will occur very quickly at the extremely high values of $T_{kin}$ calculated for the thermal nonequilibrium region of the shock layer. Park's model does not take this into account, but a related 2-T model by Losev et al.[5] does account for this rotation-vibration

24

coupling effect. In the end, however, all the 2-T models use empirical Arrhenius expressions for the dissociation reaction rate coefficients. So within a given model, the parameters of the rate coefficients are adjusted so each ad hoc 2-T model reproduces some set of data from ground tests or flight data.
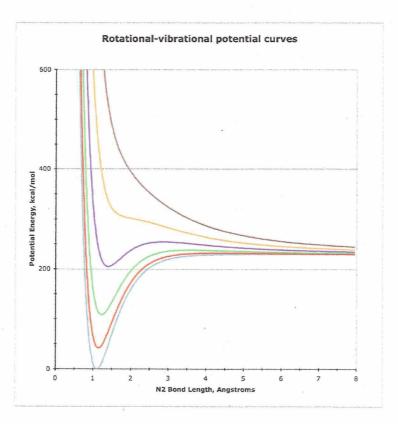


**Figure 2. Rotational-vibrational potential energy curves for $N_2$ illustrating how the vibrational potential changes with increasing rotational quantum number. The bottom curve (blue) is for J=0. As J increases, the well-depth diminishes and the centrifugal barrier at R ≈ 2.5-3.5 Å increases. For J>279, the potential becomes repulsive as seen in the top two curves (orange and brown).**

Under the aegis of the NASA/ARMD Fundamental Aerodynamics Program, we are formulating a new detailed air chemistry model based on first principles theoretical calculations that will be suitable for Earth entry at velocities of 10-14 km/s. It has long been realized that computational chemistry modeling can be used to determine the dissociation and energy transfer rates for high-temperature air under these conditions. Atomistic simulation methods for studying these collisional processes are based on classical mechanics and require knowledge of the interatomic forces acting between the collision partners (or potential energy). Until recently, these calculations used empirical potentials that were adjusted to reproduce available experimental data. For example, Billing[15], Lagana and coworkers[16,17] and most recently Esposito et al.[18,19] have used this approach to compute collision cross sections and dissociation rate coefficients for $N_2 + N_2$ and $N_2 + N$ collisions. However, with current computer resources, it is now possible to carryout these calculations without empiricism using first principles quantum chemistry methods to compute the potentials and quasiclassical trajectory methods for the simulation. As part of our work, we are computing a complete set of cross sections for rotation-vibration energy transfer in collisions of $N_2 + M$, where M = N or $N_2$. These data will be used to evaluate the relaxation and excitation rates for all rotation-vibration energy levels of $N_2$ to enable us to fully characterize the shock layer for air under hypersonic conditions. We will use these results to formulate a reduced chemical and thermodynamic model that can be used in the calculation of aerothermodynamic flowfields. In this paper we present results for rotation-vibration energy transfer in $N_2 + N$ collisions. Results for the $N_2$ dissociation reaction are given in a companion paper.[20]

## II.     Computational Approach

To study collisions between ground electronic state nitrogen atoms and molecules, we carry out simulations using classical mechanics to describe the motion of the atoms, but base these simulations on a quantum mechanical description of the forces between the atoms. For atoms heavier than hydrogen, classical mechanics has proven to be an accurate method for modeling collisions between atoms and molecules if the electronic state of the colliding species does not change. The accuracy of the results of these simulations, however, is dependent on having an accurate description for the interatomic forces, which we determine from first principles quantum mechanics calculations. In this way, the resulting characterization of the nonequilibrium $N_2$-N mixture is free from empiricism. Our overall computational approach is broken down into four steps: (1) quantum mechanics solution of the interatomic forces or the potential surface (PES) that describes the interaction energy between the three nitrogen atoms for any geometrical arrangement, (2) analytical representation of these forces for a grid of atomic positions, (3) classical mechanics simulation of $N_2$ + N collisions, and (4) reduction of the simulation data to determine rate coefficients for rotation-vibrational energy transfer and chemical reactions.

The first step is the generation of the potential energy surface that describes the forces between the nitrogen atoms. This is accomplished by solving the Schrödinger equation for the electron motion at a grid of fixed nuclear geometries: $HY = EY$ where H is the quantum Hamiltonian operator consisting of the electron kinetic energy term and coulomb potential terms for electron-electron and electron-nuclei interactions, E is the energy and Y is the wavefunction that contains information about the spatial and energy distribution of the electrons. For $N_3$, solutions are required for thousands of geometries. In general, a hierarchy of methods is used to solve the electronic problem. For a given nuclear geometry, the most computationally efficient and reliable method is used [21-23]. For all but the simplest cases, the electronic Schrödinger equation is solved by a series of numerical expansions. First, the wave function taken to be a linear combination of hydrogenic atomic orbitals, each expressed as a Gaussian function, centered on each nucleus (called the basis set). Then the electron-electron potential is simplified to so each electron experiences only the average potential of the remaining electrons (the Hartree Fock approximation) and the Schrödinger equation is solved variationally to minimize the energy E. The resulting coefficients for the Gaussian basis transform the atomic orbitals into molecular orbitals that are delocalized over all atoms. To go beyond the Hartree Fock approximation, electron correlation effects are considered whereby each electron feels the instantaneous potential of the other electrons. Electron correlation is usually introduced by mixing in a series of arrangements of electrons in the molecular orbitals (a second expansion over molecular orbitals) and solving the resulting eigenvalue problem. In the present case, the specific method employed is called CASSCF+ACPF[22,23]. We do these calculations using a large atomic orbital basis set (58 Gaussian terms for each N atom) denoted aug-cc-pvtz[24,25]. The computer code MOLPRO[26] was used for calculations, which were carried out on the Columbia supercomputer at NASA Ames Research Center. It is difficult to judge the accuracy of these quantum chemistry calculations, but based on our prior experience and comparison with well-known characteristics of the $N_2$ molecule, we believe the computed energy for each $N_3$ geometry, relative to three infinitely separated nitrogen atoms, is accurate to $\pm$ 5-10 kJ/mol or $dE/k_B < 1500$ K.

The second step is the determination of a faithful analytic representation of the energy and forces on the grid of geometries where the electronic problem was solved. This representation is known as the potential energy surface. Basic representations have been devised in the past for analogous problems. For $N_3$, the analytic representation is based on the form used by Stallcop et al. [27]. This is actually the trickiest step, because the representation must describe reproduce the quantum mechanical energies over a wide range of geometric arrangements of the atoms, and it remains the least systematized step in this work. The $N_3$ potential energy surface obtained from the above procedure is described in the next section.

In the third step, cross sections are determined by carrying out classical trajectories for $N_2$ + N collisions. In a classical trajectory calculation, classical mechanics is assumed to be a good approximation for describing individual collisions between gas-phase atoms and molecules. Large numbers of collisions are computed with randomly selected initial orientations and vibrational phase. The collision cross section for a particular process is proportional to the fraction of trajectories ending in the appropriate final state (e.g., with a certain change in the $N_2$ vibration energy). If each trajectory in a batch has the same initial molecular (v, J) level and the results are partitioned by final (v', J') level the calculations are called *Quasi Classical Trajectories (QCT)*[28,29]. For $N_2$ + N, between 1000 and 6000 trajectories were carried out for each translational energy or temperature for each of the 9390 different (v, J) levels of $N_2$. As a result of the random sampling scheme used for initial conditions of each trajectory, the statistical error associated with each computed cross section is inversely proportional to the square root of the sample size. In this study, the most of the individual state-to-state cross section values have statistical errors of

±10% or less, with the remainder having statistical errors of less than ±20%. Other sources of error are difficult to quantify and include the accuracy of the quantum chemical potential and the fidelity of the analytic fit of the PES.

The individual state-to-state cross section is $S(E_{rel},v,J,v',J')$, where $E_{rel}$ is the relative translation energy for the $N_2 + N$ collision, v and J are the initial quantum numbers, and v' and J' are the final quantum numbers. The state-to-state rate coefficient $K(v,J,v',J',T_{kin})$ is obtained by the integration of $S(E_{rel},v,J,v',J')$ with a thermal weighting in $E_{rel}$. Overall rate coefficients are obtained by summing over (v', J') and thermally averaging over the initial (v, J) levels (with the (2J+1) degeneracy factor included for rotation). For this work we use the rotation-vibration levels obtained from solutions of the Schrödinger equation for atomic motion using the WKB method[30] and based on the $N_2$ vibrational potential of LeRoy, which was determined from accurate spectroscopic analysis.[31] The fourth and final step involves analysis of the copious amount of cross section data to extract information about the overall rates of vibration and rotation energy transfer and the evolution of $T_{kin}$, $T_{rot}$ and $T_{vib}$ in the shock layer.

## III.    Results

The $N_3$ PES provides a representation of the potential energy of three nitrogen atoms in any arbitrary arrangement and geometry. For example, if the N atoms are labeled $N^a$, $N^b$ and $N^c$, the PES describes the $N^aN^b$, $N^aN^c$ and $N^bN^c$ dinitrogen molecules, separated atoms ($N^a + N^b + N^c$) and a possible triatomic complex ($N^aN^bN^c$ and its permutations). If we consider the collision between $N^a$-$N^b$(v, J) and $N^c$, the possible outcomes are $N^a$-$N^b$(v', J') + $N^c$, $N^a$-$N^c$(v', J') + $N^b$, $N^b$-$N^c$(v', J') + $N^a$ and $N^a + N^b + N^c$. The first is a nonreactive, but inelastic, collision resulting in the $N_2$ molecule having a different internal energy level and the last is dissociation of the initial $N_2$ molecule. The other two outcomes represent products of an exchange reaction where the atoms comprising the final $N_2$ molecule are different from the initial molecule. For vibration energy transfer, all possible values for $Dv = v' - v$ are considered, but for rotation, nuclear statistics dictate that only even values of DJ are allowed in nonreactive collisions (even and odd DJ are allowed for collisions resulting in exchange reaction). From spectroscopic data[31], the $N_2$ diatomic potential has its minimum at $R=R_e = 1.097679$ Å and a well depth of 955.165 kJ/mol ($D_e$ the potential energy difference between $R=R_e$ and $\infty$). For J=0, this potential has 61 vibration levels and the highest value of J for which a bound vibration level exists is J = 279. From the first principles quantum calculations, we find the energy barrier for the exchange reaction is 190.0 kJ/mol (relative to the reference geometry with $N_2$ at $R_e$ and the third N atom infinitely far away) and occurs for a N-N-N geometry with N-N bond lengths of 1.18 and 1.48 Å and a N-N-N angle of 119°. The energy where the two bond lengths are equal is 14.6 kJ/mol lower than the barrier or 175.4 kJ/mol above the reference geometry. A view of the $N_3$ PES, with the N-N-N angle fixed at 115°, is shown in Fig. 3. This PES differs in several important ways from the empirical PES used in previous QCT studies[16-19] of $N_2 + N$ collisions. That potential[16] has a much lower energy barrier for the exchange reaction (150.6 kJ/mol) and favors a collinear approach (180° N-N-N angle). These factors serve to make the exchange reaction more probable than it should be. It also uses an inferior $N_2$ vibrational potential that has 65 bound levels and a maximum rotation quantum number of 261.

Two series of QCT calculations have been carried out for $N_2$+N collisions. In the first series the translation energy was sampled from at 20,000 K thermal distribution and a batch of 6000 trajectories was run for each of the 9390 possible $N_2$ ground electronic state (v, J) levels. In the second series, the translation energy was sampled from a 60,000 K thermal distribution and 1000 trajectories for each (v, J) level considered. In the latter case, approximately 6000 (v, J) levels were included. This case mainly includes the lowest 2/3 of the set of $N_2$ energy levels as ranked by rotation-vibration energy. For both cases, the translation energy was sampled from a discrete set of 64 energies between 27.4 and 4840.0 kJ/mol with a thermal weighting factor of $E_{rel}^{1/2} \exp(-E_{rel}/k_BT)$. The individual trajectories in each set can be reweighted for a different temperature so that cross sections and rate coefficients can be computed at other temperatures as well. With the range of $E_{rel}$ values used in these calculations, we can compute energy transfer rate coefficients for $T_{kin} > 10,000$ K, but the results are not as accurate as the 20,000 K and 60,000 K values.

Typical results for vibration and rotation energy transfer rate coefficients for $N_2 + N$ at $T_{kin} = 20,000$ K are given in Fig. 4-6 and 7-8, respectively. These figures show the rate coefficients for changes in v and J for collisions of $N_2$ with initial rotation levels J = 40, 80, and 120. J = 80 has 151.36 kJ/mol rotation energy (measured for v = 0), which is close to the mean rotation energy at this temperature. Trajectories for all possible vibration levels at these values of J are included and separate values are shown for nonreactive (inelastic) and for collisions undergoing exchange reaction. In the latter, there is a greater propensity for change in the final (v, J) level. From Fig. 4 and 7, it can be seen that energy transfer is characterized by small changes in Dv and DJ: Dv = ±1 and DJ = ±2 dominate, but |DJ| < 20 have sizeable rate coefficients. For nonreactive collisions, the elastic peaks (Dv=0 and DJ=0) are much larger than the inelastic rate coefficients. As shown in Fig. 5 for vibration, Dv = ±1 ranges from about a factor of 20 lower

than Dv=0 for J= 40 to a factor of 12 lower for J=120, and the Dv = ±2 values are a factor of 2-3 lower than Dv = ±1. Fig. 6 shows the behavior of the rate coefficients for large |Dv|. It can be seen that the exchange reaction is correlates Dv < 0 and its rate coefficients are much larger for very high initial v levels, because of the large values for Dv < -30. In general, the exchange reaction serves to broaden the energy transfer distributions and make jumps of multiple vibration levels more probable. From Fig. 6 it can also be seen that the Dv distribution broadens for Dv > 0, but the opposite is true for Dv < 0. As a result there is not much difference in the width of the distributions for the three initial J values. For rotational energy transfer, the rate coefficient distributions become more narrow as J increases from 40 to 120 and remain almost symmetric about DJ=0, as shown in Fig. 8b. Rate coefficients for the exchange reaction contribute equally to both positive and negative DJ up to DJ = ±40. Thus, large changes in the rotation energy level are probable in a single collision.

The rate coefficients for rotation and vibration energy transfer at 20,000 K are compared in Fig. 9 for initial J = 40, 80 and 120. The rate coefficients for DJ are consistently larger than those for Dv, but only by a factor of 2-5. This is most easily seen for the J = 80 case (the red and blue lines in the figure).
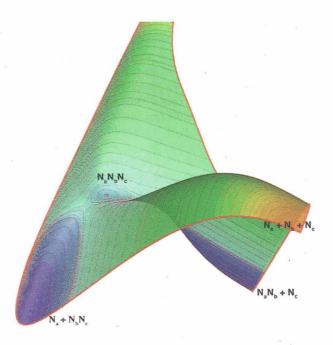


**Figure 3. Representation of the $N_3$ potential energy surface with the N-N-N angle constrained to 115°. Blue regions have low energy and orange/red regions have high energy. The potential energy minima corresponding to $N^a + N^bN^c$ and $N^aN^b + N^c$ are shown. These arrangements are connected by a reaction path for the exchange reaction which has a barrier and shallow minimum labeled $N^aN^bN^c$. The energy surface shown is an analytical fit based on first principles quantum chemistry calculations.**

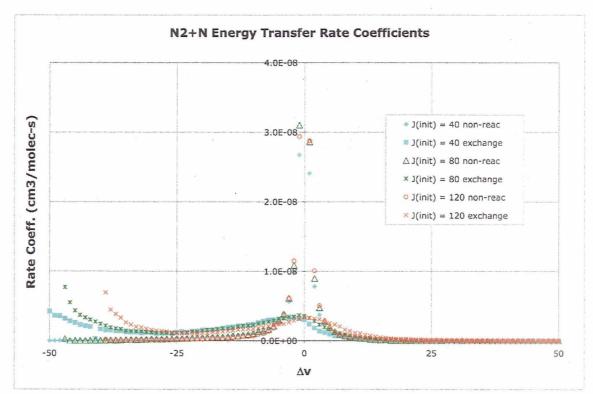**N2+N Energy Transfer Rate Coefficients**

Figure 4. Overview of rate coefficients for vibration energy transfer at $T_{kin}$ = 20,000 K for fixed initial rotation quantum numbers: J = 40, 80 and 120.

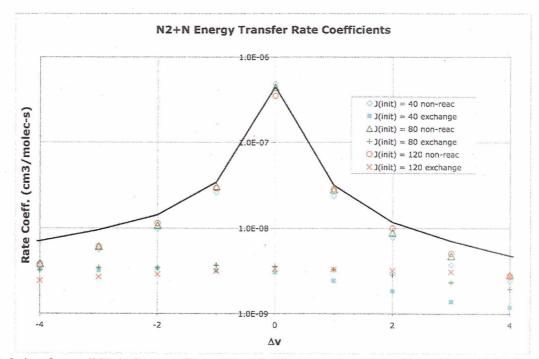**N2+N Energy Transfer Rate Coefficients**

Figure 5. Detailed view for small |Dv| of rate coefficients for vibration energy transfer at $T_{kin}$ = 20,000 K for fixed initial rotation quantum number. The black line is the total rate coefficient (nonreactive plus exchange) for J = 80.

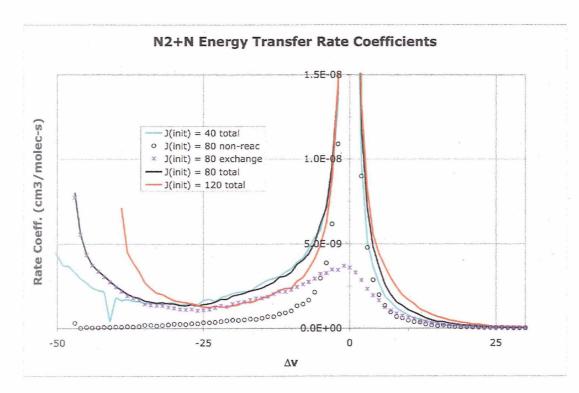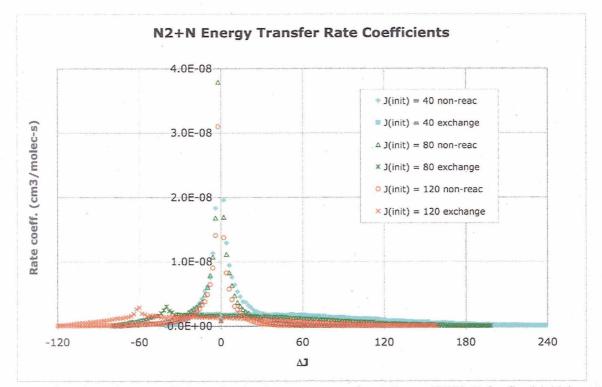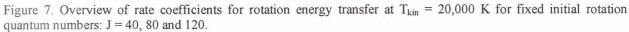**N2+N Energy Transfer Rate Coefficients**



Figure 6. Rate coefficients for vibration energy transfer at $T_{kin} = 20,000$ K for fixed initial rotation quantum number: detailed view for large |Dv| showing the importance of the exchange reaction.

**N2+N Energy Transfer Rate Coefficients**



Figure 7. Overview of rate coefficients for rotation energy transfer at $T_{kin} = 20,000$ K for fixed initial rotation quantum numbers: J = 40, 80 and 120.
   a.

## N2+N Energy Transfer Rate Coefficients
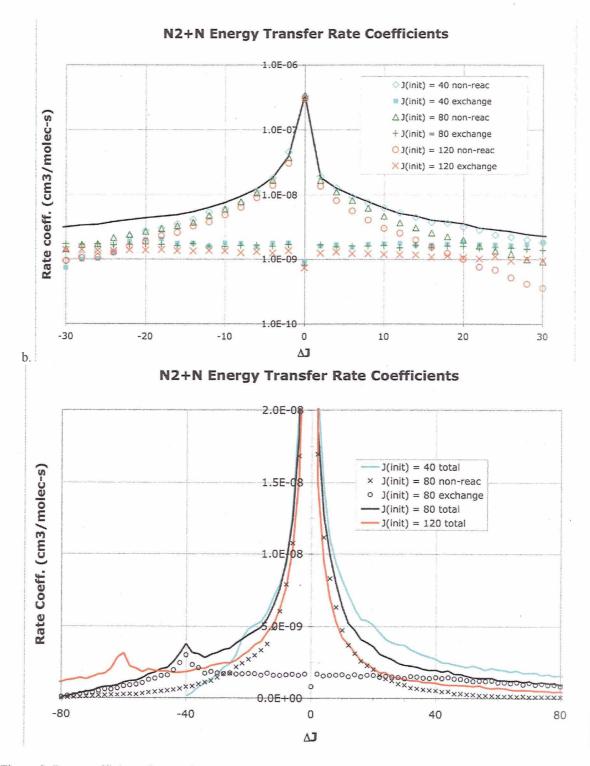


b.

## N2+N Energy Transfer Rate Coefficients



Figure 8. Rate coefficients for rotation energy transfer at $T_{kin}$ = 20,000 K for fixed initial rotation quantum number. (a) Detailed view for small |DJ|. The black line is the total rate coefficient (nonreactive plus exchange) for J = 80. (b) Detailed view for large |DJ| showing the importance of the exchange reaction.

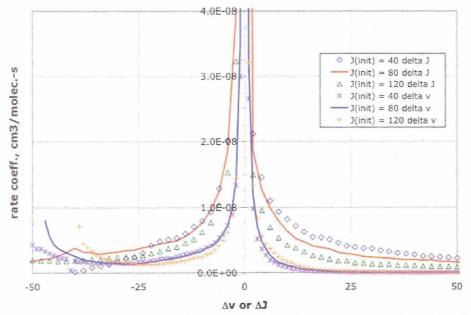**Comparison of rate coefficients for Δv and ΔJ**



Figure 9. Comparison of rate coefficients for rotation and vibration energy transfer at $T_{kin}$ = 20,000 K for fixed initial rotation quatum number.

Selected rate coefficients are computed for vibrational energy transfer for $T_{rot}$ = $T_{kin}$ between 10,000 K and 60,000 K. As mentioned above, the thermal sampling for $E_{rel}$ is not appropriate for lower temperatures. However, our interest is in understanding the physics and chemistry of the nonequilibrium region of the shock layer, which is characterized by this range of kinetic temperature. For the case of v = 5 (Fig. 10) we compare rate coefficients for vibrational excitation and relaxation (Dv = +1 and -1, respectively) as well as Dv = +5, 10 and 30. It can be seen that the rate coefficients for inelastic collisions are about five times larger than for exchange reaction for Dv = +1, but for Dv = 5 they are comparable and for Dv = 10 and 30 the rate coefficient for exchange is much larger than for inelastic collisions. In addition, the rate coefficients for Dv = +1 and -1 are nearly identical. In Fig. 11 we compare rate coefficients for Dv = +1 for initial v = 0, 1, 2, 3, and 5. It can be seen that the rate coefficients for inelastic trajectories have nearly the same value as do the rate coefficients for the exchange reaction. In addition, the ratio of inelastic to exchange rate coefficients is approximately 10 throughout the temperature range and for all initial v's. The corresponding rate coefficients computed for Trot = 10,000 K instead of $T_{rot}$ = $T_{kin}$ were almost indistinguishable from the data presented in Fig. 10. Thus, the details of the vibrational energy transfer rates are not affected by the choice of $T_{rot}$. We cannot make detailed comparison with the previous QCT studies using the empirical PES[16-19], because the maximum $T_{kin}$ used in that work is between 4000 K and 10,000 K. At $T_{kin}$ = 10,000 K, however, the magnitudes of the rate coefficients in [19] are comparable to data shown in Fig. 10 and 11.
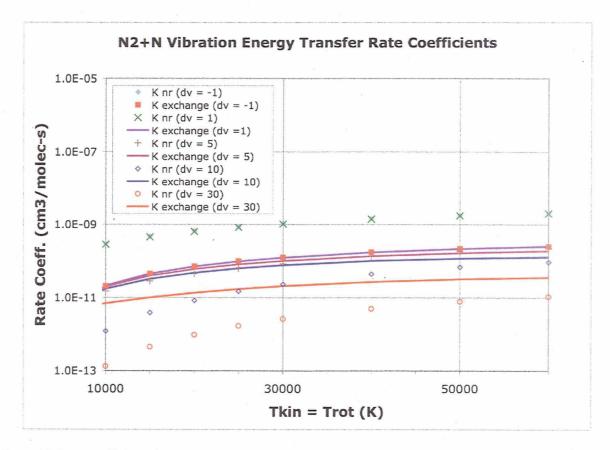
Figure 10. Rate coefficients for vibrational energy transfer in $N_2(v=5)$ due to collisions with N atoms as a function of $T_{kin} = T_{rot}$.
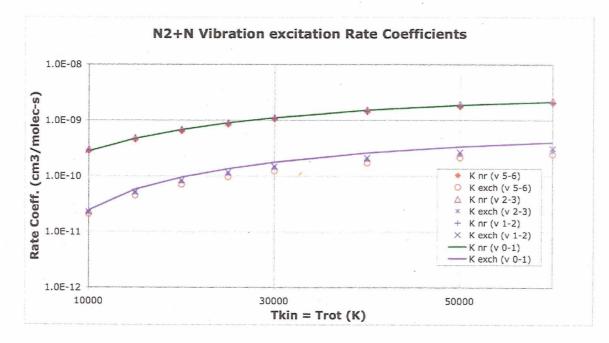


Figure 11. Rate coefficients for vibrational energy excitation ($\Delta v = +1$) in $N_2(v=0,1,2,5)$ due to collisions with N atoms as a function of $T_{kin} = T_{rot}$.

# IV.    Summary

We have presented rate coefficients for the excitation of vibrational and rotational energy in shock heated $N_2$ at temperatures between 10,000 and 60,000 K due to collisions with N atoms. These data are based on first principles theoretical calculations, using classical mechanics to simulate individual collisions of $N_2$ with N, and a quantum chemical potential energy surface to describe the interatomic forces experienced by the collision partners. The resulting rate coefficients for rotational and vibrational energy transfer demonstrate the importance of exchange reactions (where the initial and final $N_2$ molecules are comprised of different nitrogen atoms), because they result in multiquantum changes in vibration and rotation quantum number and serve to hasten the equilibration of vibration and kinetic temperature. These results will be combined with a similar study of $N_2 + N_2$ collisions (in progress) to characterize the shock layer around spacecraft re-entering Earth's atmosphere.

## Acknowledgments

## References

[1]. C. Park, "Nonequilibrium hypersonic aerothermodynamics", Wiley, New York (1989).

[2]. C. Park, "Assessment of a two-temperature model for dissociating and weakly ionizing nitrogen", J. Thermophysics and Heat Transfer 2, 8-16 (1988).

[3]. C. Park, "Review of chemical-kinetic problems for future NASA missions, I. Earth entries", J. Thermophysics and Heat Transfer 7, 385-398 (1993).

[4]. C. Park, R. L. Jaffe and H. Partridge, "Chemical-kinetics parameters for hyperbolic Earth entry", J. Thermophysics and Heat Transfer 15, 76-90 (2001).

[5]. S. A. Losev, V. N. Makarov, M. J. Pogosbekyan, O. P. Shatalov and V. S. Nikol'sky, "Thermochemical nonequilibrium kinetic models in strong shock waves on air", AIAA-94-1990.

[6]. L. Landau and E. Teller, "Theory of sound dispersion", Physikaliche Zeit. Der Sowjetunion 10, 34-43 (1936).

[7]. R. N. Schwartz, Z. I. Slawsky and K. F. Herzfeld, "Calculation of vibrational relaxation times in gases", J. Chem. Phys. 22, 767-773, (1954).

[8]. I.V. Adamovich, S.O. Marcheret, J.W. Rich, and C.E. Treanor, "Non-perturbative analytic theory of V-T and V-V rates in diatomic gases, including multi-quantum transitions", AIAA-95-2060.

[9]. I.V. Adamovich, "Three dimensional analytic model of vibrational energy transfer in molecule-molecule collisions", AIAA Journal 39, 1916-1925 (2001).

[10]. R.C. Millikan and D.R. White, "Systematics in vibrational relaxation". J. Chem. Phys. 39, 3209-3213 (1963).

[11]. D. Giordano, "On the statistical and axiomatic thermodynamics of multitemperature gas mixtures", Doctoral thisis, Universite de Provence, 2005.

[12]. The average temperature was first defined as $(T_{kin}T_{vib})^{1/2}$[2], but was later generalized[3].

[13]. R.L. Jaffe, "Rate constants for chemical reactions in high-temperature nonequilibrium air", in Progress in Astronautics and aeronautics, Vol 103,Thermphysical aspects of re-entry flows, J.N. Moss and C.D. Scott, eds. AIAA, NY, 1986, pp 123-151.

[14]. A.A. Vigasin, "Thermally averaged effective dissociation energy of dimers", Chem. Phys. Lett. 242, 33-38 (1995).

[15]. G.D. Billing and E.R. Fisher, "VV and VT rate coefficients in $N_2$ by a quantum-classical model", Chem. Phys. 43, 395-401 (1979).

[16]. A. Lagana, E. Garcia and L. Ciccarelli, "Deactivation of vibrationally excited nitrogen molecules by collision with nitrogen atoms", J. Phys. Chem. 91, 312-314 (1987).

[17]. A. Lagana and E. Garcia, "Temperature dependence of N + $N_2$ rate coefficients", J. Phys. Chem. 98, 502-507 (1994).

[18]. F. Esposito, M. Capitelli and C. Gorse, "Quasi-classical dynamics and vibrational kinetics of N + $N_2$(v) system", Chem. Phys. 257, 193-202 (2000).

[19]. F. Esposito and M. Capitelli, "QCT calculations for the process $N_2$(v) + N → $N_2$(v') + N in the whole temperature range", Chem. Phys. Lett. 418, 581-585 (2006).

[20]. D.W. Schwenke, G. Chaban, R. Jaffe and W. Huo "Dissociation cross sections and rate coefficients for nitrogen from accurate theoretical calculations", AIAA-2008-1209.

[21]. G. D. Purvis and R. J. Bartlett, "A Full Coupled-cluster Singles and Doubles Model: The Inclusion of Disconnected Triples", J. Chem. Phys. 76 (2), 1910-1918 (1982).

[22]. K. Raghavachari, G. W. Trucks, J. A. Pople, and M. Head-Gordon, "A Fifth-order Perturbation Comparison of Electron Correlation Theories", Chem. Phys. Lett. 157 (5), 479-483 (1989).

[23]. R.J. Gdanitz and R. Ahlrichs, "The averaged coupled-pair functional (ACPF): A size-extensive modification of MR CI(SD)", Chem. Phys. Lett. 143 (4), 413-420 (1988).

[24]. T. H. Dunning, J. Chem. Phys. 90, 1007 (1989).

[25]. R.A. Kendall, T.H. Dunning and R.J. Harrison, J. Chem. Phys. 96, 6796 (1992).

[26] MOLPRO is a package of *ab initio* quantum chemistry programs written by  H.-J. Werner, and P. Knowles with contributions from R.D. Amos, A. Bernhardsson, A. Berning et al

[27]. D. Wang, J.R. Stallcop, W. M. Huo, C. E. Dateo, D. W. Schwenke, and H. Partridge, "Quantal Study of the Exchange Reaction for N + $N_2$ using an *ab initio* potential energy surface", J. Chem. Phys. **118** (3), 2186-2189 (2003).

[28]. D. W. Schwenke, "Calculation of rate constants for the three-body recombination of $H_2$ in the presence of $H_2$", J. Chem. Phys. **89**, 2076-2091 (1988).

[29]. D. G. Truhlar and J. T. Muckerman, " Reactive Scattering Cross Sections: Quasiclassical and Semiclassical Methods", in "Atom-Molecule Collision Theory", Ed. by R. B. Bernstein (Plenum, New York, 1979) p. 505-566.

[30]. D.W. Schwenke, "Calculation of rate constants for the three-body recombination recombination of $H_2$ in the presence of $H_2$", J. Chem. Phys. **89** (2), 2076-2091 (1988).

[31]. R.J. LeRoy, Y. Huang and C. Jary, "An accurate analytic potential function for ground-state $N_2$ from a direct-potential-fit analysis of spectroscopic data", J. Chem. Phys. **125**, 164310 (2006).